Bone 120 (2019) 176–186

Contents lists available at ScienceDirect

Bone

journal homepage: www.elsevier.com/locate/bone

Full Length Article

Sphenoid bone hypoplasia is a skeletal phenotype of cleidocranial dysplasia in a mouse model and patients

Keisuke Mitomo[a,b], Satoru Matsunaga[b,c,d], Kei Kitamura[b,e], Takashi Nakamura[b,f], Akiko Saito[f], Toshihisa Komori[g], Takashi Muramatsu[a,b,d], Akira Yamaguchi[b,d,*]

[a] Department of Operative Dentistry, Cariology and Dental Pulp Biology, Tokyo Dental College, Tokyo, Japan
[b] Tokyo Dental College Research Branding Project, Tokyo Dental College, Tokyo, Japan
[c] Department of Anatomy, Tokyo Dental College, Tokyo, Japan
[d] Oral Health Science Center, Tokyo Dental College, Tokyo, Japan
[e] Department of Histology, Tokyo Dental College, Tokyo, Japan
[f] Department of Biochemistry, Tokyo Dental College, Tokyo, Japan
[g] Department of Cell Biology, Nagasaki University Graduate School of Biomedical Sciences, Nagasaki, Japan

ARTICLE INFO

Keywords:
Cleidocranial dysplasia
Sphenoid bone
Runx2
Osterix
Secondary cartilage

ABSTRACT

Cleidocranial dysplasia (CCD) is an autosomal dominant disorder caused by heterozygous mutations in *RUNX2*. Affected individuals exhibit delayed maturation or hypoplasia in various bones, mainly including those formed by intramembranous ossification. Although several reports described deformation of the sphenoid bone in CCD patients, details of the associated changes have not been well documented. Most parts of the sphenoid bone are formed by endochondral ossification; however, the medial pterygoid process is formed by intramembranous ossification associated with secondary cartilage. We first investigated histological changes in the medial pterygoid process during different developmental stages in *Runx2*$^{+/+}$ and *Runx2*$^{+/-}$ mice, finding that mesenchymal cell condensation of the anlage of this structure was delayed in *Runx2*$^{+/-}$ mice as compared with that in *Runx2*$^{+/+}$ mice. Additionally, in *Runx2*$^{+/+}$ mice, Osterix-positive osteoblastic cells appeared at the upper region of the anlage of the medial pterygoid process, and bone trabeculae appeared to associate with subsequent secondary cartilage formation. By contrast, few Osterix-positive osteoblastic cells appeared at the upper region of the anlage of the medial pterygoid process, and no bone trabeculae appeared thereafter in *Runx2*$^{+/-}$ mice. At more advanced embryonic stages, endochondral ossification occurred at the lower part of the medial pterygoid process in both *Runx2*$^{+/+}$ and *Runx2*$^{+/-}$ mice. After birth, well-developed bone trabeculae occupied two-thirds of the cranial side of the medial pterygoid process, and cartilage appeared beneath these bones in *Runx2*$^{+/+}$ mice, whereas thin trabecular bone appeared at the center of the cartilage of the medial pterygoid process in *Runx2*$^{+/-}$ mice. In adult mice, the body and medial pterygoid processes of the sphenoid bone comprised mature bones in both *Runx2*$^{+/+}$ and *Runx2*$^{+/-}$ mice, although the axial length of the medial pterygoid processes was apparently lower in *Runx2*$^{+/-}$mice as compared with that in *Runx2*$^{+/+}$mice based on histological and micro-computed tomography (CT) examinations. Moreover, medical-CT examination revealed that in CCD patients, the medial pterygoid process of sphenoid bone was significantly shorter relative to that in healthy young adults. These results demonstrated that the medial pterygoid process of the sphenoid bone specifically exhibited hypoplasia in CCD.

1. Introduction

Mammalian skeletons are formed by two essential patterns: intramembranous and endochondral ossifications [1,2]. Intramembranous ossification is achieved by the direct transformation of mesenchymal cells into osteoblasts, with parts of the skull, maxilla, mandible, and pelvis formed by this ossification pattern. During endochondral ossification, chondrocytes that differentiated from mesenchymal cells first form the cartilage template (primary cartilage) for each skeletal tissue, which is replaced by bone after cartilage mineralization. Various axial and appendicular bones, vertebral columns, sternums, and ribs are formed by this process. Some bones are formed

* Corresponding author at: Oral Health Science Center, Tokyo Dental College, 2-9-8 Kanda Misakicho, Chiyoda-ku, Tokyo 101-0061, Japan.
E-mail address: akira@tdc.ac.jp (A. Yamaguchi).

https://doi.org/10.1016/j.bone.2018.10.028
Received 10 August 2018; Received in revised form 31 October 2018; Accepted 31 October 2018
Available online 02 November 2018
8756-3282/

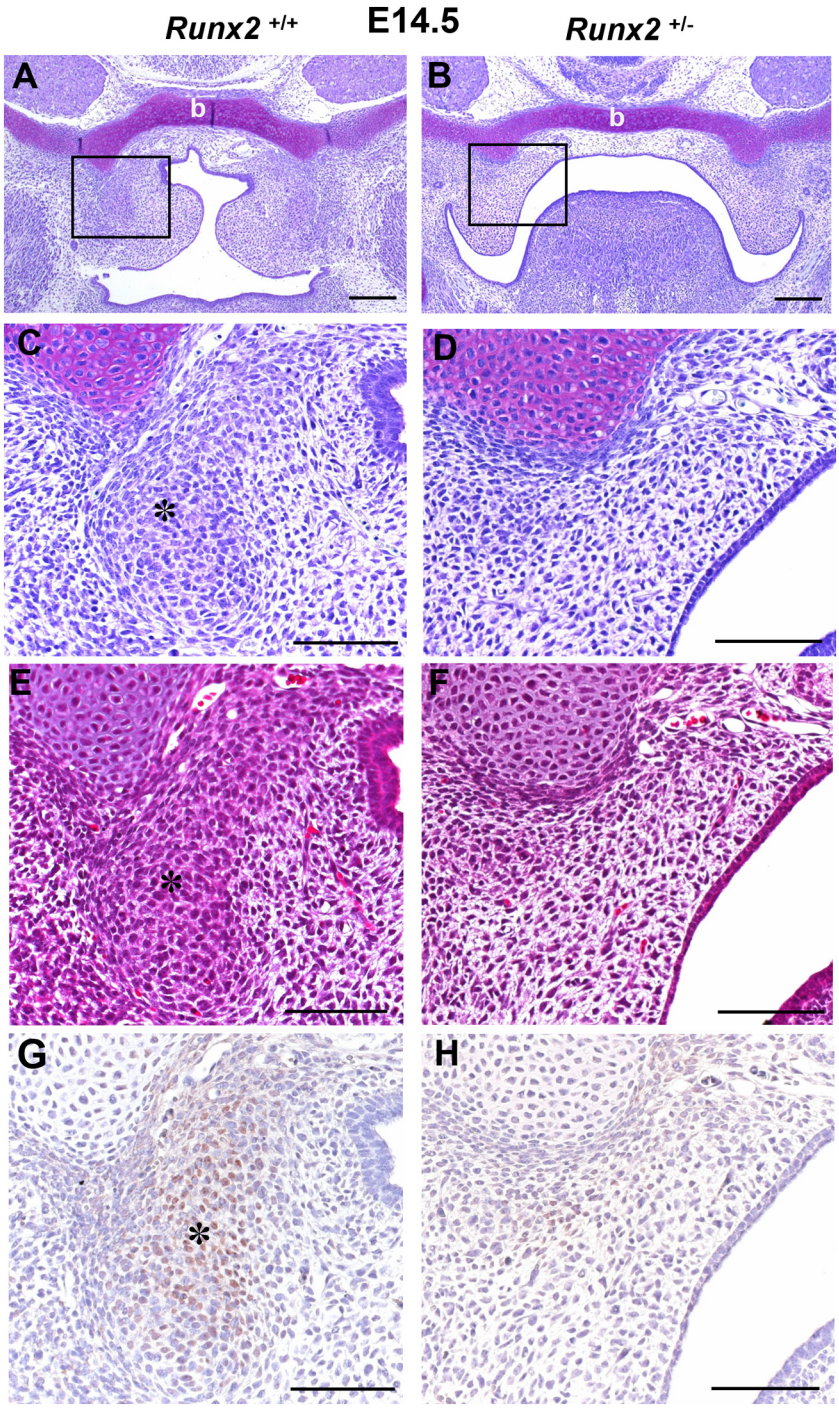

Fig. 1. Histology of the medial pterygoid process region of sphenoid bone in *Runx2*$^{+/+}$ (A, C, E, and G) and *Runx2*$^{+/-}$ (B, D, F, and H) mice on embryonic day 14.5. (A, B) Overall histology of the sphenoid bone and surrounding tissues. The body (b) of sphenoid bone comprises cartilage in both mice, and the anlage of the medial pterygoid process is observed as mesenchymal cell condensation (asterisk) beneath the lateral end of the sphenoid body in *Runx2*$^{+/+}$ mice (C, E, and G), whereas this is not observed in *Runx2*$^{+/-}$mice (D, F, and H). (C, E, and G; and D, F, and H) Higher magnifications of regions denoted in (A) and (B), respectively. Osterix-positive cells are scattered throughout the region of mesenchymal cell condensation in *Runx2*$^{+/+}$ mice (G), although few Osterix-positive cells are observed in *Runx2*$^{+/-}$ mice (H). (A–D), Toluidine blue staining, (E, F) hematoxylin and eosin staining, and (G, H) immunohistochemistry for Osterix. Black bars represent 200 μm (A, B) and 100 μm (C–H).

by a combination of the two ossification patterns, including the lateral end of the clavicle, which is formed by intramembranous ossification while the medial part is formed by endochondral ossification [3–5].

Runt-related transcription factor 2 (Runx2) is a key transcription factor that regulates osteoblast differentiation [6–8] and plays essential roles in bone formation during both intramembranous and endochondral ossification [9,10]. Cleidocranial dysplasia (CCD) is an autosomal dominant disorder caused by heterozygous mutations in *RUNX2*, which is located on chromosome 6p21 [1,2,11–15]. Affected individuals exhibit delayed maturation or hypoplasia in various skeletal tissues that form mainly via intramembranous ossification. Among these, delayed closure of fontanels and cranial sutures, Wormian bones (intra sutural bones), brachycephaly, depressed nasal bridge, supernumerary teeth, delayed eruption of permanent teeth, and hypoplasia or aplasia of the clavicle are common features observed in patients with CCD [1,11–15].

Although mice with *Runx2* homozygous mutation (*Runx2*$^{-/-}$) die immediately after birth without breathing due to a complete lack of bone formation [6,7], *Runx2* heterozygous mice (*Runx2*$^{+/-}$) reach adulthood but exhibit a skeletal phenotype similar to that observed in CCD patients, except for changes in the teeth [6]. These results indicate that *Runx2*$^{+/-}$ mice represent an ideal animal model for exploring skeletal changes that occur in CCD.

Primary cartilage appears at the cartilage anlage before undergoing endochondral ossification. In addition to this tissue, some cartilage in the maxillofacial region and clavicle is referred to as secondary

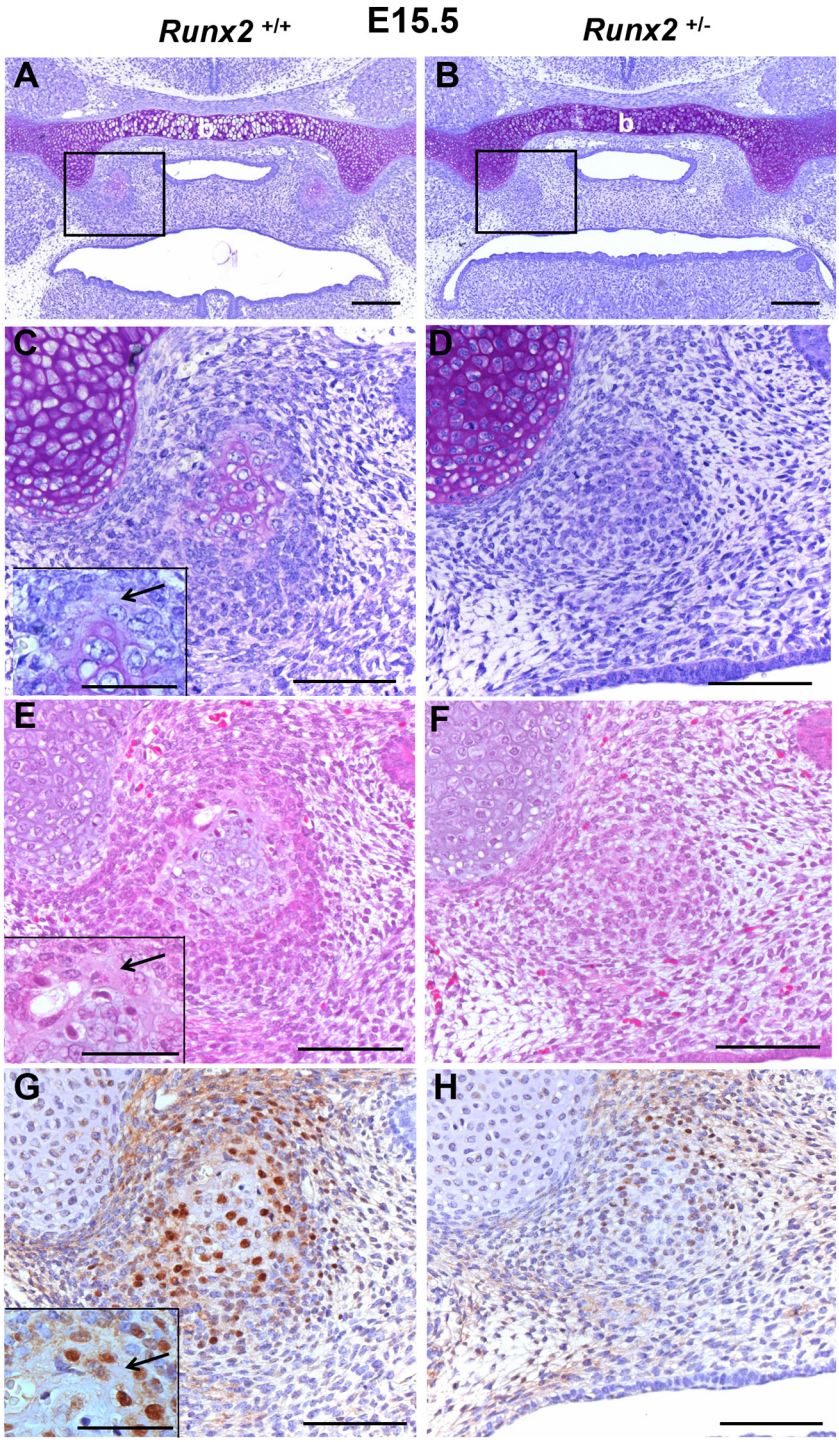

Fig. 2. Histology of the medial pterygoid process region of sphenoid bone in *Runx2*$^{+/+}$ (A, C, E, G) and *Runx2*$^{+/-}$ (B, D, F, H) mice on embryonic day 15.5. (A, B) Overall histology of the sphenoid bone and surrounding tissues. Hypertrophy of chondrocytes in the body (b) of the sphenoid bone in *Runx2*$^{+/+}$ mice (A) is enhanced as compare with that observed in *Runx2*$^{+/-}$ mice (B). (C, E, and G; and D, F, and H) Higher magnification of regions in (A) and (B), respectively. The bone matrix (arrow) appears at the upper area of the medial pterygoid process in *Runx2*$^{+/+}$ mice. (C, E, and G; inserts) Higher magnification of the bone matrix. (G) Numerous Osterix-positive cells are scattered throughout the medial pterygoid process region. (H) No bone formation appears at the medial pterygoid process, and several Osterix-positive cells are observed in the upper area of the medial pterygoid process. Toluidine blue staining (A–D), hematoxylin and eosin staining (E, F), and immunohistochemistry for Osterix (G, H). Black bars represent 200 μm (A, B), 100 μm (C–H), and 50 μm (C, E, and G; inserts).

cartilage, because it arises from the periosteum of previously formed bones [2,16–19], with mandibular condylar cartilage, mandibular angular cartilage, mandibular coronoid cartilage, and lateral cartilage of the clavicle belonging to this category [18,20–22]. We previously reported that cartilage types of the sphenoid bone are classified into different two classes, based on the aforementioned categories during developmental stages: the lateral pterygoid process belongs to the class of primary cartilage, whereas the medial pterygoid process comprises secondary cartilage. Specifically, the lateral pterygoid process is formed by endochondral ossification while the medial pterygoid process is initially formed by intramembranous ossification associated with subsequent secondary cartilage [21,22].

Therefore, the sphenoid bone is formed by a combination of endochondral and intramembranous ossification similar to that observed with the clavicle. Most of the sphenoid bone is ossified by endochondral ossification; however, the upper part of the medial pterygoid process is first formed by intramembranous ossification associated with the secondary cartilage [21,22]. Because the skeletal tissues formed by intramembranous ossification are severely affected in CCD patients and mouse models [1,23,24], it is worthwhile to investigate whether the development of the medial pterygoid process of sphenoid bone is affected by CCD. Although several reports described deformation of the sphenoid bone in CCD patients based on the examination of cephalometric radiographs [13,25,26], the details of these morphological

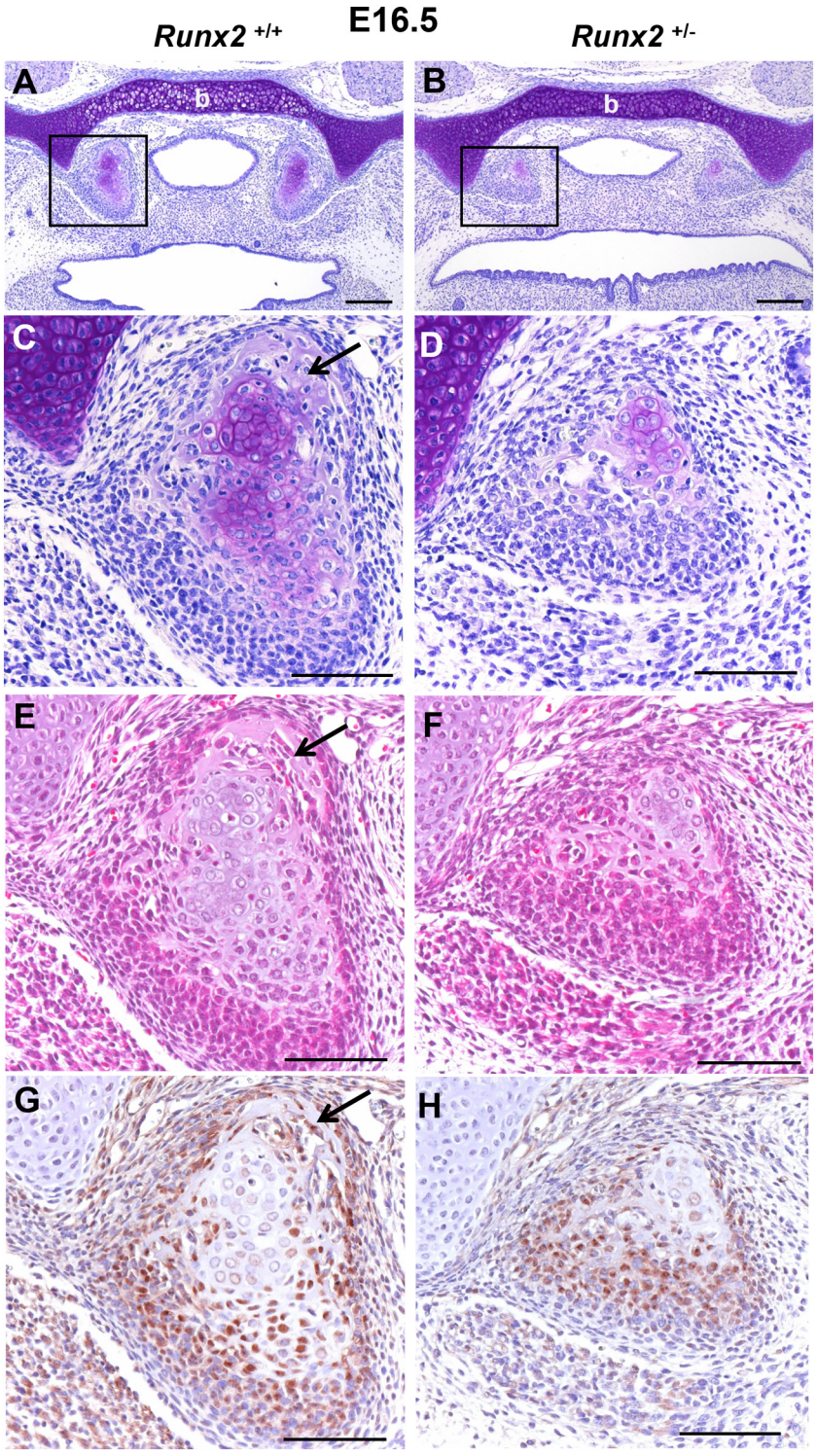

Fig. 3. Histology of the medial pterygoid process region of sphenoid bone in *Runx2*$^{+/+}$ (A, C, E, and G) and *Runx2*$^{+/-}$ (B, D, F, and H) mice on embryonic day 16.5. (A, B) Overall histology of the sphenoid bone and surrounding tissues. Increased progression of chondrocyte hypertrophy in the body (b) of the sphenoid bone in *Runx2*$^{+/+}$ mice (A) relative to that observed in *Runx2*$^{+/-}$ mice (B). (C, E, and G; and D, F, and H) Higher magnification of regions in (A) and (B), respectively. Bone trabeculae (arrow) appear at the upper area of the medial pterygoid process, and cartilage formed beneath these trabecular bones and the lower part of the medial pterygoid process in *Runx2*$^{+/+}$ mice (C, E, and G). Numerous Osterix-positive cells are scattered around the trabecular bones and the cartilage at the lower part of the medial pterygoid process region (G). Cartilage appears at the center of the medial pterygoid process and is associated with no apparent bone formation (D, F). Osterix-positive cells mainly distribute beneath the cartilage and observed at the medial pterygoid process (H). Toluidine blue staining (A–D), hematoxylin and eosin staining (E, F), and immunohistochemistry for Osterix (G, H). Black bars represent 200 μm (A, B), and 100 μm (C–H), respectively.

changes have not been well documented. Furthermore, few reports have described morphological changes in the sphenoid bone in mouse models of CCD. Therefore, we conducted an extensive investigation of the morphological changes that occur in the sphenoid bone in CCD using a mouse model and patients.

In this study, we showed that the medial pterygoid process of the sphenoid bone, which is first formed by intramembranous ossification associated with secondary cartilage, exhibited hypoplasia in a mouse model of CCD and in patients. This represents the first study demonstrating that the sphenoid bone is a distinct target of CCD.

2. Materials and methods

2.1. Experimental animals

All mice were housed in animal facilities approved by the Nagasaki University and Tokyo Dental College, respectively. All experiments were reviewed and approved by the Animal Care and Use Committee of Nagasaki University Graduate School of Biomedical Sciences (No. 1403111129-21) and Tokyo Dental College (No. 300402).

Mouse embryos obtained from *Runx2*$^{+/+}$ and *Runx2*$^{+/-}$ pregnant

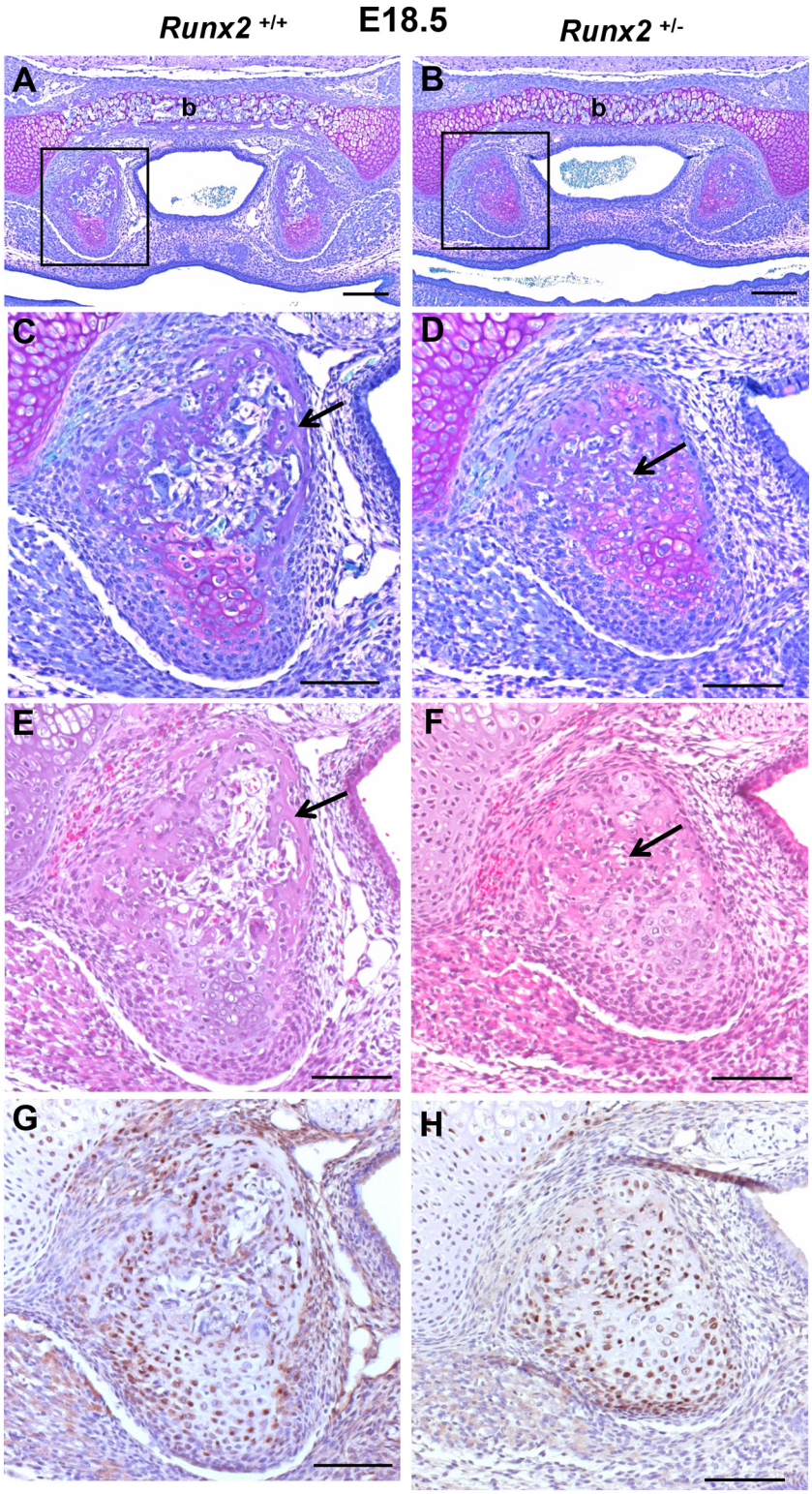

Fig. 4. Histology of the medial pterygoid process region of sphenoid bone in *Runx2*$^{+/+}$ (A, C, E, and G) and *Runx2*$^{+/-}$ (B, D, F, and H) mice on embryonic day 18.5. (A, B) Overall histology of the sphenoid bone and surrounding tissues. Chondrocyte hypertrophy in the body (b) of the sphenoid bone is similar between *Runx2*$^{+/+}$ mice (A) and *Runx2*$^{+/-}$ mice (B). (C, E, and G; and D, F, and H) Higher magnification of regions in (A) and (B), respectively. Bone trabeculae (arrow) associated with bone marrow occupies the upper two-thirds, and cartilage occupies the lower one-third of the medial pterygoid process in *Runx2*$^{+/+}$ mice (C, E). Numerous Osterix-positive cells are scattered around the trabecular bones and beneath the cartilage in the lower part of the medial pterygoid process region (G). Bone trabeculae (arrow) appear at the medial pterygoid process region, but are located in the central area of the cartilage comprising the medial pterygoid process in *Runx2*$^{+/-}$ mice (D, F). Osterix-positive cells are mainly distributed at the central area and beneath the cartilage (H). Toluidine blue staining (A–D), hematoxylin and eosin staining (E, F), and immunohistochemistry for Osterix (G, H). Black bars represent 200 μm (A, B), and 100 μm (C–H).

mice (gestational days 14.5, 15.5, 16.5, and 18.5) and those from newborn mice (postnatal day 3) were used to explore histological changes at each developmental stage. Ten *Runx2*$^{+/+}$ and eight *Runx2*$^{+/-}$ mice at 10 weeks of age were also used to investigate the sphenoid bone in adult animals. These mice were used for subsequent experiments after euthanasia with diethyl ether.

2.2. Histological observation

The skulls isolated from embryonic, newborn, and adult *Runx2*$^{+/+}$ and *Runx2*$^{+/-}$ mice were fixed in 4% paraformaldehyde in phosphate-buffered saline (PBS) followed by decalcification with 10% ethylenediaminetetraacetic acid. They were then embedded in paraffin, and 5-μm-thick serial frontal or sagittal sections were prepared from each paraffin block. These sections were stained with 0.05% toluidine blue in PBS (pH 7.2) and hematoxylin and eosin, as well as for

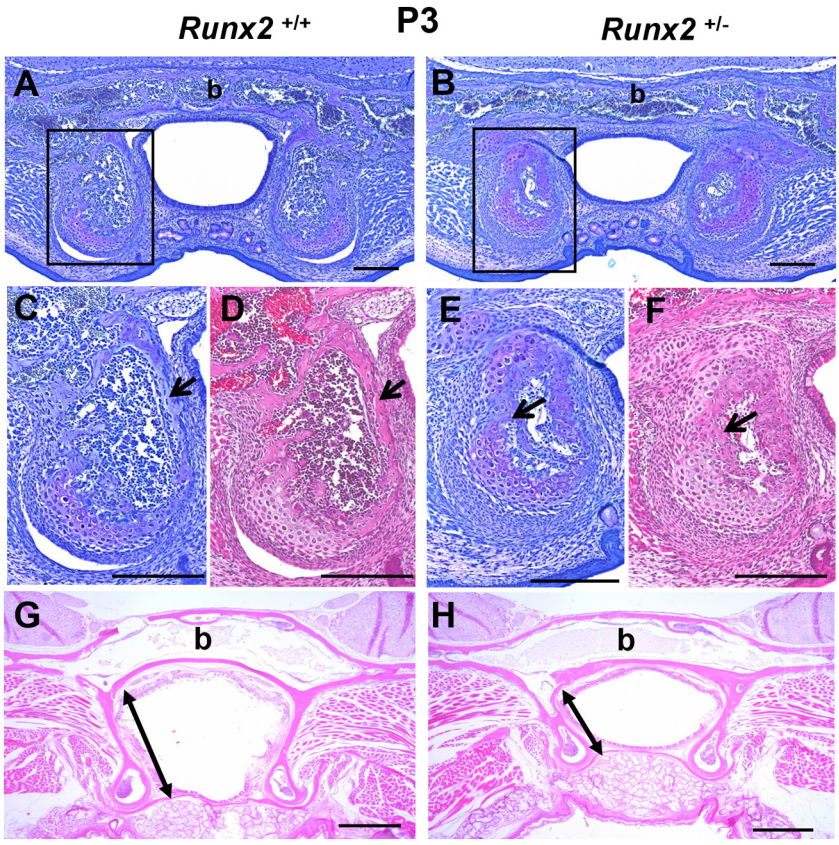

Fig. 5. Histology of the medial pterygoid process region of the sphenoid bone in *Runx2*$^{+/+}$ (A, C, D, and G) and *Runx2*$^{+/-}$ (B, E, F, and H) mice on postnatal day 3. (A, B) Overall histology of the sphenoid bone and surrounding tissues. Bone tissue replaces the body of the sphenoid bone (b) and is associated with bone marrow formation, in both *Runx2*$^{+/+}$ (A) and *Runx2*$^{+/-}$ (B) mice. (C, D; and E, F) Higher magnification images of regions in (A) and (B), respectively. Bone trabeculae (arrows) associated with bone marrow occupy the upper three-quarters, and cartilage occupiy the lower one-quarter of the medial pterygoid process in *Runx2*$^{+/+}$ mice (C, D). Bone tissue (arrows) appears at the central region surrounded by cartilage of the medial pterygoid process in *Runx2*$^{+/-}$ mice (E, F). Histology of the sphenoid bone in 10-week-old *Runx2*$^{+/+}$ (G) and *Runx2*$^{+/-}$ (H) mice. The body of the sphenoid bone (b) is completely replaced by bone, and the medial pterygoid process (doubled-heads arrows) in *Runx2*$^{+/-}$ (H) mice is shorter than that in *Runx2*$^{+/+}$ (G) mice. Toluidine blue (A–C, E) and hematoxylin and eosin staining (D, F–H). Black bars represent 200 μm (A–F) and 500 μm (G, H).

immunohistochemical staining. At least four *Runx2*$^{+/+}$ and *Runx2*$^{+/-}$ embryos and newborn mice were used for histological investigation.

2.3. Immunohistochemical analysis

We investigated the expression of Osterix (Sp7) by immunohistochemistry. After deparaffinization, sections mounted on the slides were incubated with 0.3% hydrogen peroxide in methanol for 30 min, followed by several washes in PBS and incubation with 3% bovine serum albumin for 1 h to block nonspecific binding. The sections were subsequently treated with an anti-Sp7/Osterix antibody (ab22552; Abcam, Cambridge, UK) for 1 h at 37 °C in a moisture chamber. After washing with PBS, a secondary antibody was applied using EnVision+ Dual Link (DAKO, Santa Clara, CA USA) at room temperature. After several washes with PBS, the sections were treated with ImmPACT DAB substrate (Funakoshi, Tokyo, Japan) to detect any reaction, followed by inspected after counterstaining with hematoxylin.

2.4. Analysis of murine sphenoid bone by micro-computed tomography

Skulls isolated from adult *Runx2*$^{+/+}$ and *Runx2*$^{+/-}$ mice (10-week-old) were used to obtain micro-CT images using a micro-CT system (HMX-225 Actis4, Tesco Co., Tokyo, Japan). Based on these data, two-dimensional slice data were prepared using the back-projection method. Three-dimensional (3D) images were constructed based on the volume-rendering method from slice data using analytical software (TRI/3D-BON; RATOC System Engineering Co., Tokyo, Japan). After observing the basic structure of bones in the skulls, we conducted more precise analysis of the medial pterygoid process of sphenoid bone. To quantitatively assess the size of the process, we measured the lengths of medial pterygoid processes from the frontal, axial, and sagittal planes of the 3D images. For frontal sections, the length of the medial pterygoid process was defined by measuring the length of a perpendicular line from the tip of the medial pterygoid process to the skull base line. For axial sections, the length was defined by measuring the distance from the tip to the base of the medial pterygoid process. The sagittal section was used to measure the length of the pterygoid hamulus of the medial pterygoid process. For these measurements, the longest distance from the serial CT images was chosen as the length of each medial pterygoid process and pterygoid hamulus.

2.5. CCD patients

Experimental procedures applied to healthy young adults and CCD patients were approved by the Ethics Committee of Tokyo Dental College (permit no. 533). All patients provided written informed consent before participating in the study.

We enrolled four CCD patients (11–27 years of age; average:18.5 years) who had visited Suidobashi Hospital or Chiba Dental Center of Tokyo Dental College in order to analyze the structure of craniofacial skeletons by medical CT. Four young adults who had no craniofacial bone symptoms (16–27 years of age; average: 21.2 years) were used as healthy controls. A heterozygous *RUNX2* mutation in CCD patients was confirmed by sequence analysis of genomic DNA extracted using an Easy-DNA™ gDNA purification kit (Thermo Fisher Scientific, Waltham, MA, USA). Mutations in CCD1 and CCD2 were determined, as reported previously [27], and mutations in CCD3 and CCD4 were analyzed by exome sequence using an Illumina Hiseq 2500 (Illumina, San Diego, CA, USA). Sequence mapping and mutation analysis were performed, as described previously [28].

2.6. Analysis of human sphenoid pterygoid processes by CT

The morphology of sphenoid bone in CCD patients and healthy young adults was observed by medical CT (SOMATOM Definition AS; Siemens, Erlangen, Germany). Using 3D-structure-analysis software (Mimics 19.0; Materialise, Leuven, Belgium), 3D- reconstructed images were prepared, and the inner structure was observed. For frontal

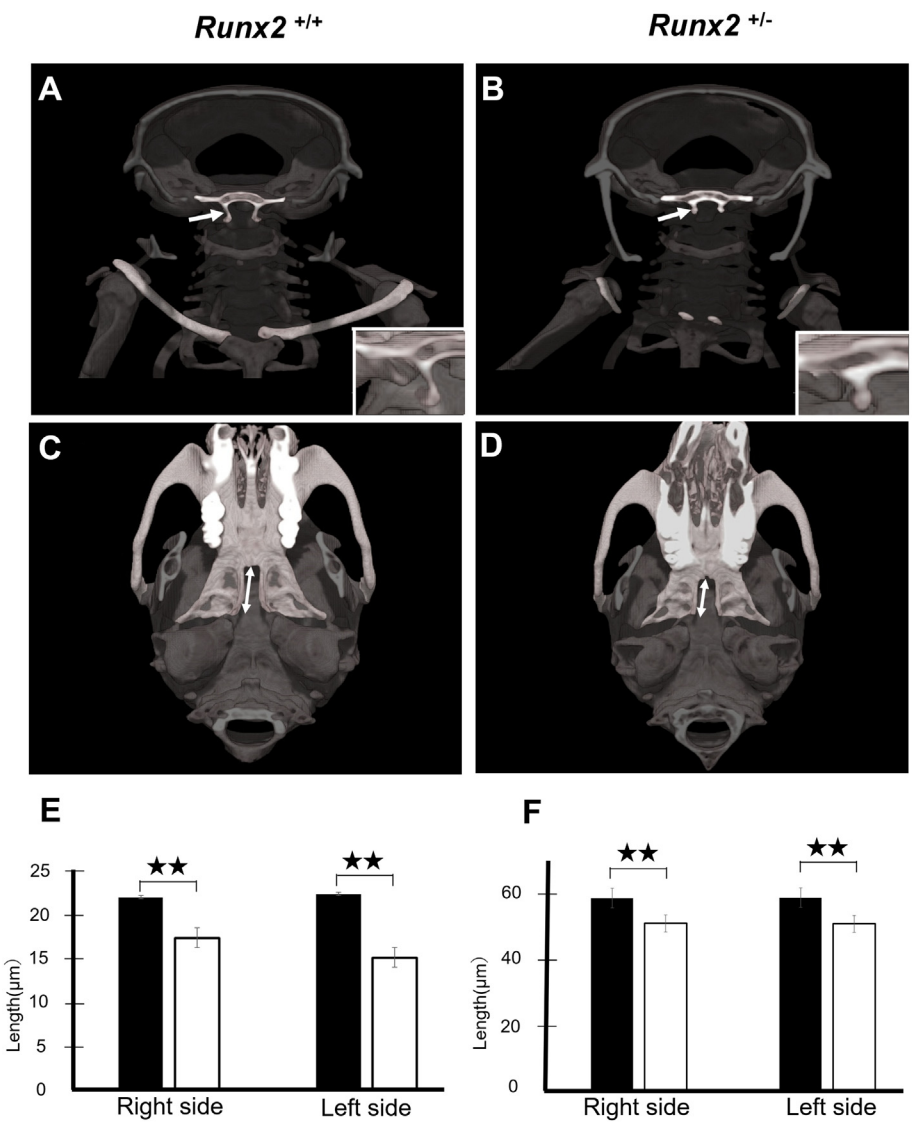

Fig. 6. Micro-CT analyses of sphenoid bones in *Runx2*$^{+/+}$ (A, C) and *Runx2*$^{+/-}$ (B, D) mice. Frontal (A, B) and axial (C, D) 3D images constructed from micro-CT data, with sphenoid bone highlighted in each image. Measurement of the lengths of the medial pterygoid processes (white arrows) in *Runx2*$^{+/+}$ (A) and *Runx2*$^{+/-}$ (B) mice. Inserts indicate higher magnification images for each mouse. The clavicle is normal in *Runx2*$^{+/+}$ mice (A), but hypoplastic in *Runx2*$^{+/-}$ mice (B). Measurement of the front-occipital lengths of the medial pterygoid processes (double-headed white arrows) in *Runx2*$^{+/+}$ (C) and *Runx2*$^{+/-}$ (D) mice. Quantitative valuation of the lengths of the medial pterygoid processes on both sides of the frontal (E) and axial (F) sections in *Runx2*$^{+/+}$ (black bars) and *Runx2*$^{+/-}$ (white bars) mice. ($n = 10$ for the *Runx2*$^{+/+}$ group; and ($n = 8$)for the *Runx2*$^{+/-}$ group; $P < 0.01$).

Table 1
Clinical symptoms and gene mutations in CCD patients and healthy control.

	Symptoms	CCD1	CCD2	CCD3	CCD4	HC1	HC2	HC3	HC4
Age		23	13	27	11	27	22	16	20
Gender		Female	Female	Male	Female	Male	Male	Male	Female
Craniofacial	Patency of the anterior fontanelle	○	○	○	○	—	—	—	—
	Delation of cranial suture	○	○	○	○	—	—	—	—
	Wormian bone	○	○	○	○	—	—	—	—
	Hypoplasia of nasal bone	○	○	○	○	—	—	—	—
Tooth	Multiple supernumerary teeth	○	○	○	○	—	—	—	—
	Retention of permanent teeth	○	○	○	○	—	—	—	—
General	Hypoplasia of clavicle	○	○	○	○	—	—	—	—
	Short stature	○	—	X	—	—	—	—	—
	Family history	—	—	X	—	—	—	—	—
Mutation		R391X a	Q67Xa	R190Q	K134E	✻	✻	✻	✻

○: Exhibition of symptoms, —: No symptom, X: not available, ✻: no examination, a: these mutations were reported previously [27].

images, the entire image of the medial pterygoid process was observed based on serial slices of sphenoid bone, and the maximum length was extracted in each case. Because CCD patients often present shorter heads, manifesting as a larger cephalic index (the ratio of the maximum width of the head × 100/the maximum length), we normalized the length of the medial pterygoid process to the distance between both foramen ovale.

2.7. Statistical analysis

An unpaired Student's *t*-test was used for statistical comparisons, and $P < 0.01$ was considered significant.

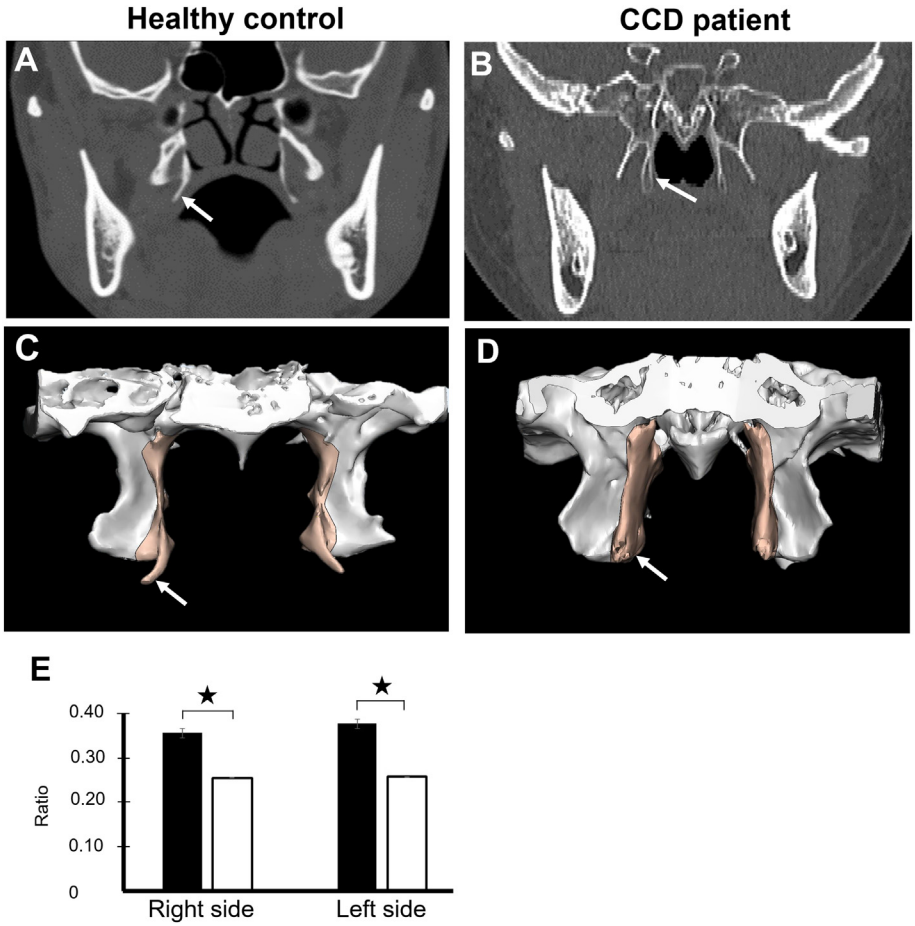

Fig. 7. Frontal medical-CT images of the craniofacial region of a healthy young adult (A) and CCD patient (B). White arrows indicate the medial pterygoid processes of the sphenoid bones. (C, D) 3D-reconstructed images of the sphenoid bone in a healthy young adult (C) and CCD patient (D). The medial pterygoid process is emphasized in a bronze color. Hypoplasia is more prominent in the pterygoid hamulus (white arrows) of CCD patients (D) as compared with that observed in healthy young adults (C). (E) The length of the medial pterygoid process of both sides in healthy young adults (black bars) and CCD patients (white bars) ($n = 4$ for both groups; $P < 0.05$).

3. Results

3.1. Comparison of histological changes in the medial pterygoid process of the sphenoid bone during different developmental stages between *Runx2*$^{+/+}$ and *Runx2*$^{+/-}$ mice

In both *Runx2*$^{+/+}$ and *Runx2*$^{+/-}$ mice, the cartilage core appeared at the body of the sphenoid bone by embryonic day 14.5 (Fig. 1). Mesenchymal cell condensation was evident at the area that forms the future medial pterygoid process in *Runx2*$^{+/+}$ mice, whereas this was not apparent in *Runx2*$^{+/-}$ mice (Fig. 1A, C, E and G). These areas showed no apparent metachromasia based on toluidine blue staining in both wild type and heterozygous mice (Fig. 1 C and D). In *Runx2*$^{+/+}$ mice, many Osterix-positive cells were distributed at the region of mesenchymal-cell condensation (Fig. 1G), whereas few Osterix-positive cells appeared in the same area in *Runx2*$^{+/-}$ mice (Fig. 1H).

On embryonic day 15.5, cartilage of the sphenoid body in *Runx2*$^{+/+}$mice was more hypertrophic than that in *Runx2*$^{+/-}$ mice (Fig. 2A and B), and mesenchymal cells at the cranial side of the future medial pterygoid process formed an osteoid lacking definite metachromasia in *Runx2*$^{+/+}$ mice (Fig. 2C, E, and G; arrows). In these areas, many Osterix-positive cells were scattered around the osteoid, small flattened cells located at the cranial region of mesenchymal-cell condensation were also positive for Osterix in *Runx2*$^{+/+}$ mice (Fig. 2G). In *Runx2*$^{+/-}$ mice, mesenchymal-cell condensation appeared at the future medial pterygoid process (Fig. 2B, and D), and a small number of Osterix-positive cells was scattered at the cranial region of mesenchymal-cell condensation (Fig. 2H), although no osteoid formation was observed (Fig. 2F). Furthermore, no metachromasia was observed in sites of mesenchymal cell condensation in *Runx2*$^{+/-}$ mice (Fig. 2D).

On embryonic day 16.5, cartilage hypertrophy in the sphenoid body of *Runx2*$^{+/+}$mice preceded that observed in *Runx2*$^{+/-}$ mice (Fig. 3A, and B), and the cranial site of the medial pterygoid process was covered by the bone collar comprising thin trabeculae (Fig. 3C, E, and G). Additionally cartilage exhibiting strong metachromasia appeared beneath the bone collar and the lower part of the medial pterygoid process in *Runx2*$^{+/+}$ mice (Fig. 3C); with Osterix-positive cells distributed around the bone collar and the lower region of the cartilage (Fig. 3G). In *Runx2*$^{+/-}$ mice, cartilage that exhibited weak metachromasia appeared at the central region of the site of mesenchymal-cell condensation (Fig. 3D), with no bone collar comprising thin trabeculae observed at the cranial site of the medial pterygoid process (Fig. 3F). Additionally, Osterix-positive cells were distributed in the lower part of the cartilage at sites of mesenchymal-cell condensation (Fig. 3H).

On embryonic day 18.5, hypertrophic cartilage occupied the sphenoid body in both *Runx2*$^{+/+}$ and *Runx2*$^{+/-}$ mice (Fig. 4A, and B), and the upper two-thirds of the cranial side of the medial pterygoid process comprised trabecular bones associated with Osterix-positive cells and bone marrow in *Runx2*$^{+/+}$ mice (Fig. 4C, E, and G). We observed mature cartilage in one-third of the oral site of the medial pterygoid process region, with Osterix-positive cells also distributed in the lower part of the cartilage (Fig. 4C, E, and G). In *Runx2*$^{+/-}$ mice, the bone collar covering the cranial region of the cartilage was not observed (Fig. 4D, and F), and osteoid-like tissue associated with Osterix-positive cells appeared at the center of the cartilage core along with Osterix-positive cells appearing at the lower part of the cartilage (Fig. 4H).

On day 3 after birth, well-developed bone trabeculae associated with bone marrow were observed in two-thirds of the cranial side of the medial pterygoid process region, and cartilage was observed beneath these bones in *Runx2*$^{+/+}$ mice (Fig. 5A, C, and D). By contrast, thin trabecular bone associated with bone marrow cells appeared at the center of the cartilage at the medial pterygoid process region in

Runx2$^{+/-}$ mice (Fig. 5E, and F).

In adult mice, the body and the medial pterygoid processes of the sphenoid bone comprised mature bones with bone marrow in both *Runx2*$^{+/+}$ and *Runx2*$^{+/-}$ mice as a result of the complete replacement of cartilage (Fig. 5G, and H). However, the axial length of the medial pterygoid processes of the sphenoid bone in *Runx2*$^{+/-}$ mice was apparently shorter than that in *Runx2*$^{+/+}$ mice (Fig. 5G, and H).

3.2. Comparison of the medial pterygoid process of the sphenoid bone by micro-CT analysis between *Runx2*$^{+/+}$ and *Runx2*$^{+/-}$ mice

Fig. 6 shows typical micro-CT images of the craniofacial and clavicular regions of 10-week-old *Runx2*$^{+/+}$ and *Runx2*$^{+/-}$ mice, with the structures of the sphenoid bones and clavicles highlighted for clarification. The medial pterygoid processes of the sphenoid bone in *Runx2*$^{+/-}$ mice were shorter than those in *Runx2*$^{+/+}$ mice based on both the frontal and axial planes (Fig. 6A–D arrows). Additionally, 3D-reconstructed features of the medial pterygoid processes of the sphenoid bone revealed clearly shorter structures in *Runx2*$^{+/-}$ mice (Fig. 6A and B; inserts), axial images revealed hypoplasia of the clavicles (Fig. 6A, and B). Moreover we observed a shorter structure of the pterygoid hamulus in sagittal sections in *Runx2*$^{+/-}$ mice (Fig. S1A, and B).

We then measured the length of the medial pterygoid processes of the sphenoid bone based on micro-CT images from the frontal and axial planes by using the 3D-reconstructed model of the sagittal sections. The medial pterygoid processes on the right and left sides in *Runx2*$^{+/-}$ mice were significantly shorter than those in *Runx2*$^{+/+}$ mice based on measurements of both frontal and axial sections (Fig. 6E, and F). Additionally, the pterygoid hamulus in sagittal sections was significantly shorter in *Runx2*$^{+/-}$ mice, relative to that observed in *Runx2*$^{+/+}$ mice (Fig. S1C).

3.3. Clinical symptoms and gene mutations in CCD patients

Table 1 summarizes the clinical symptoms, including X-ray findings and genetic mutations in CCD patients. All patients presented sufficient symptoms associated with clinical CCD, and heterozygous mutations were confirmed in the *RUNX2* gene based on sequence analysis of genomic DNA. Moreover, we identified a different mutation in each of the four patients (CCD1; R391X [27], CCD2; Q67X [27], CCD3; R190Q, CCD4; K134E) in exons 1through 7 of the *RUNX2* gene (Table 1).

3.4. Analyses of the medial pterygoid process of the sphenoid bone in patients with CCD

Fig. 7 shows typical medical-CT images of the frontal planes of normal young adults (Fig. 7A) and CCD patients (Fig. 7B). As indicated by white arrows, the medial pterygoid processes of the sphenoid bone in CCD patients were shorter as compared to those in normal young adults. We then measured the length of the medial pterygoid processes of the sphenoid bone in normal young adults and CCD patients based on their frontal images, revealing that the medial pterygoid processes on both sides in CCD patients were significantly shorter than those in normal adults (Fig. 7E).

The CT images of the frontal planes (Fig. 7A, and B) suggested a lack of a pterygoid hamulus in CCD patients. To confirm these changes, we observed the medial pterygoid processes of the sphenoid bone using 3D-reconstructed images (Fig. 7C, and D), which verified the absence of the pterygoid hamulus in CCD patients.

4. Discussion

In this study, we compared developmental changes in the medial pterygoid process of the sphenoid bone between *Runx2*$^{+/+}$ and *Runx2*$^{+/-}$ mice. Our findings revealed that the appearance of mesenchymal cell condensation at the anlage of the medial pterygoid process was apparently delayed in *Runx2*$^{+/-}$mice as compared with that in *Runx2*$^{+/+}$ mice, suggesting that haploinsufficiency of *Runx2* reduced mesenchymal cell proliferation and migration at the anlage of the medial pterygoid process. However, further investigation is necessary to confirm these findings because Pratap et al. [29] proposed a cell-growth-suppressive function for Runx2 in bone cell progenitors.

In *Runx2*$^{+/+}$ mice, the mesenchymal cell population included numerous Osterix-positive cells, whereas this number was reduced on embryonic day 14.5 in *Runx2*$^{+/-}$ mice. Additionally, the temporal and spatial regulation of bone deposition at the medial pterygoid process differed between *Runx2*$^{+/+}$ and *Runx2*$^{+/-}$ mice across different developmental stages. In *Runx2*$^{+/+}$ mice, bone deposition first appeared as a bone collar at the cranial site of mesenchymal cell condensation associated with Osterix-positive cells on embryonic day 15.5, which was involved in secondary cartilage formation beneath the bone collar. Thereafter, cartilage appeared at the lower part of the medial pterygoid process, and numerous Osterix-positive cells appeared beneath the cartilage, suggesting the initiation of endochondral ossification in these areas. Therefore, the cranial region of the medial pterygoid process generated a bone collar and secondary cartilage, and endochondral ossification occurred at the lower part of the medial pterygoid process [21,22]. Because *Runx2*$^{+/-}$ mice lacked bone deposition as a bone collar at the cranial side of the primordial medial pterygoid process, it is possible that cartilage might appear directly at the center of the site of mesenchymal cells. In this case, Osterix-positive cells were located adjacent to the lower part of the cartilage, indicating the initiation of endochondral ossification. These data indicated that *Runx2*$^{+/-}$ mice lacked a bone collar at the cranial site of the medial pterygoid process due to the disturbance of intramembranous ossification, whereas endochondral ossification progressed even in these mice. This interpretation was further supported by histological findings observed in newborn mice (3 days old), where the medial pterygoid process was clearly divided into two layers comprising bone tissue at the cranial site and cartilage tissue in the lower part in *Runx2*$^{+/+}$ mice. By contrast, bone tissue was located in the center of the cartilage in *Runx2*$^{+/-}$ mice, indicating that this bone was formed through endochondral ossification by primary cartilage.

Recent studies characterized of secondary cartilage, which was described in detail in a classic review by Beresford [3] As including mandibular condylar cartilage, mandibular angular cartilage, coronoid cartilage, and lateral cartilage of the clavicle. Here and in our previous reports [21,22], we confirmed that the medial pterygoid process of the sphenoid bone represents secondary cartilage. Interestingly, Shibata et al. [30] revealed that Runx2-deficient mice lack mandibular condylar cartilage, indicating that Runx2 is essential for the formation of condylar cartilage, which is generated from the periosteum of previously existing bone. The lateral part of the clavicle also comprises secondary cartilage, which might be closely related to hypoplasia of the clavicle observed in CCD model mice and CCD patients. Here, we revealed hypoplasia of the medial pterygoid process of the sphenoid bone, which also belongs to the class of secondary cartilage. These findings suggested that cartilage or bones that originate from secondary cartilage are targets for CCD due to the incomplete formation of the periosteum as the origin of secondary cartilage formation.

Our results revealed that the expression of Osterix, a transcriptional factor required for osteoblast differentiation [31], was first observed in the anlage of the medial pterygoid process and subsequently distributed in the cranial region of the medial pterygoid process, where the original bone collar appears as the source of secondary cartilage in *Runx2*$^{+/+}$ mice. This phenotype was absent in *Runx2*$^{+/-}$ mice and might be closely related to the lack of a bone collar at the cranial region of the medial pterygoid process. However, many Osterix-positive cells were distributed beneath the cartilage at the lower part of the medial pterygoid process, where endochondral ossification progressed, in both *Runx2*$^{+/+}$ and *Runx2*$^{+/-}$ mice. Because Osterix participates in

stimulation of osteoblast differentiation, even in the absence of Runx2 [32,33], endochondral ossification occurred in both *Runx2*$^{+/+}$ and *Runx2*$^{+/-}$ mice. Accordingly, further investigation of the role of Osterix in secondary cartilage formation is required, because Osterix is essential for the coupling of terminal cartilage differentiation and endochondral ossification in mandibular cartilage [34], which represents a type of secondary cartilage [18,20].

We observed either hypoplasia or absence of the pterygoid hamulus in CCD model mice and CCD patients. The tensor veli palatine muscle originates from the scaphoid fossa at the posterior margin of the medial pterygoid process of the sphenoid bone and is inserted into the palatine aponeurosis located just beneath the medial pterygoid process [35,36]. These structures play important roles in nasopharyngeal closure during swallowing. During this process, the pterygoid hamulus acts as a pulley to induce smooth movement of the tensor veli palatine muscle. Medical CT observations in the present study revealed absence or hypoplasia of the pterygoid hamulus in CCD patients, although these patients harbored the scaphoid fossa at the medial pterygoid process. These findings suggested that CCD patients retain the tensor veli palatine muscle between the scaphoid fossa and palate aponeurosis, although its movement might be disturbed by the lack of a suitable pulley during swallowing. Because some CCD patients report dysphagia [37], more extensive and careful clinical studies should be performed to confirm whether this symptom is a commonly observed in CCD patients.

5. Conclusion

In this study, we showed that the medial pterygoid process of the sphenoid bone, which is formed by intramembranous ossification, represents a distinct skeletal tissue affected by CCD. Our findings suggested that more critical and careful examination of the sphenoid bone is necessary to understand the detailed pathophysiology and mechanism underlying the associated functional disturbance in CCD patients with these investigations currently ongoing in our group.

Acknowledgements

We thank Drs. Kenji Sueishi, Toshifumi Azuma, Shin-ichi Abe of Tokyo Dental College for their helpful advices and critical discussion. This research is supported by grants for Private University Branding Project supported by Ministry of Education, Culture, Sports, Science and Technology, Japan, and Tokyo Dental College Branding Project for Multidisciplinary Research Center for Jaw Disease (MRCJD): Achieving Longevity and Sustainability by Comprehensive Reconstruction of Oral and Maxillofacial functions.

Authors' roles

Study design: KM and AY. Study conduct: KM, SH, KK, TN, AS, TK. Data analysis: KM, SM, KK, AS. Drafting manuscript: KM and AY.

Appendix A. Supplementary data

Supplementary data to this article can be found online at https://doi.org/10.1016/j.bone.2018.10.028.

References

[1] M.M. Cohen, Biology of Runx2 and cleidocranial dysplasia, J. Craniofac. Surg. 24 (2013) 130–133.
[2] A.D. Berendsen, B.R. Olsen, Bone development, Bone 80 (2015) 14–18.
[3] W.A. Beresford, Chondroid Bone, Secondary Cartilage and Metaplasia, Urban & Schwarzenbang, Baltimore, 1981.
[4] L.F. Huang, H. Fukai, P.B. Selby, B.R. Olsen, S. Mundlos, Mouse clavicular development: analysis of wild-type and cleidocranial dysplasia mutant mice, Dev. Dyn. 210 (1997) 33–40.
[5] M.M. Cohen, The new bone biology: pathologic, molecular, and clinical correlates, Am. J. Med. Genet. A 140 (2006) 2646–2706.
[6] T. Komori, H. Yagi, S. Nomura, A. Yamaguchi, K. Sasaki, K. Deguchi, Y. Shimizu, R.T. Bronson, Y.H. Gao, M. Inada, M. Sato, R. Okamoto, Y. Kitamura, S. Yoshiki, T. Kishimoto, Targeted disruption of Cbfa1 results in a complete lack of bone formation owing to maturational arrest of osteoblasts, Cell 89 (1997) 755–764.
[7] F. Otto, A.P. Thornell, T. Crompton, A. Denzel, K.C. Gilmour, I.R. Rosewell, G.W. Stamp, R.S. Beddington, S. Mundlos, B.R. Olsen, P.B. Selby, M.J. Owen, Cbfa1, a candidate gene for cleidocranial dysplasia syndrome, is essential for osteoblast differentiation and bone development, Cell 89 (1997) 765–771.
[8] A. Yamaguchi, T. Komori, T. Suda, Regulation of osteoblast differentiation mediated by bone morphogenetic proteins, hedgehogs, and Cbfa1, Endocr. Rev. 21 (2000) 393–411.
[9] C.A. Yoshida, H. Yamamoto, T. Fujita, T. Furuichi, K. Ito, K. Inoue, K. Yamana, A. Zanma, K. Takada, Y. Ito, T. Komori, Runx2 and Runx3 are essential for chondrocyte maturation, and Runx2 regulates limb growth through induction of Indian hedgehog, Genes Dev. 18 (2004) 952–963.
[10] T. Komori, Runx2, an inducer of osteoblast and chondrocyte differentiation, Histochem. Cell Biol. 149 (218) (2018) 313–323.
[11] S. Mundlos, F. Otto, C. Mundlos, J. Mulliken, A. Aylsworth, S. Albright, D. Lindhout, W.G. Cole, W. Henn, J.H. Knoll, M.J. Owen, R. Mertelsmann, B.U. Zabel, B.R. Olsen, BR, mutations involving the transcription factor CBFA1 cause cleidocranial dysplasia, Cell 89 (1997) 773–779.
[12] F. Otto, H. Kanegane, S. Mundlos, Mutations in the RUNX2 gene in patients with cleidocranial dysplasia, Hum. Mutat. 19 (2002) 209–216.
[13] A.A. Kaissi, F.B. Chehida, V. Kenis, Broad spectrum of skeletal malformation complex in patients with cleidocranial dysplasia syndrome: radiographic and tomographic study, Clin. Med. Insights. Arthritis. Musculoskelet. Disord. 6 (2013) 45–55.
[14] A. Aruga, E. Hordyjewska, G. Kandzierski, P. Tylzanowski, Cleidocranial dysplasia and RUNX2-clinical phenotype-genotype correlation, Clin. Genet. 90 (2016) 393–402.
[15] E. Farrow, R. Nicot, A.A. Wiss, A. Laborde, J. Ferri, Cleidocranial dysplasia: a review of clinical, radiological, genetic implications and a guidelines proposal, J. Craniofac. Surg. 29 (2018) 382–389.
[16] H. Vinkka, Secondary cartilages in the facial skeleton of the rat, Proc. Finn. Dent. Soc. 78 (Suppl. 7) (1982) 1–37.
[17] H. Vinkka-Puhakka, I. Thesleff, Initiation of secondary cartilage in the mandible of the Syrian hamster in the absence of muscle function, Arch. Oral Biol. 38 (1993) 49–54.
[18] S. Shibata, S. Suzuki, T. Tengan, M. Ishii, T. Kuroda, A histological study of the developing condylar cartilage of the fetal mouse mandible using coronal sections, Arch. Oral Biol. 41 (1996) 47–54.
[19] T. Miyame, A.M. Cameron, B.K. Hall, Stage-specific expression patterns of alkaline phosphatase during development of the first arch skeleton in inbred C57BL/6 mouse embryos, J. Anat. 190 (1997) 239–260.
[20] T. Shibata, Y. Fujimori, Y. Yamashita, An in situ hybridization and histochemical study of development and postnatal changes of mouse mandibular angular cartilage compared with condylar cartilage, J. Med. Dent. Sci. 53 (2006) 41–50.
[21] M. Yamamoto, K. Kitamura, M. Kasahara, M. Serikawa, S. Katumura, T. Yoshimoto, T. Matubayashi, K. Odaka, S. Matsunaga, S. Abe, Histological study of the developing pterygoid process of the fetal mouse sphenoid, Anat. Sci. Int. 92 (2017) 364–372.
[22] H. Hirouchi, K. Kitamura, M. Yamamoto, K. Odaka, S. Matsunaga, K. Sakiyama, S. Abe, Developmental characteristics of secondary cartilage in the mandibular condyle and sphenoid bone in mice, Arch. Oral Biol. 89 (2018) 84–92.
[23] R.B. Martins, R.S. de Souza, E.M. Giovani, Cleidocranial dysplasia: report of six clinical cases, Spec. Care Dentist. 34 (2014) 144–150.
[24] T. Takarada, R. Nakazato, A. Tsuchikane, K. Fujikawa, T. Iezaki, Y. Yoneda, E. Hinoi, Genetic analysis of Runx2 function during intramembranous ossification, Development 143 (2016) 211–218.
[25] B.L. Jensen, S. Kreiborg, Development of the skull in infants with cleidocranial dysplasia, J. Craniofac. Genet. Dev. Biol. 13 (1993) 89–97.
[26] I. Golan, U. Baumert, B.P. Hrala, Early craniofacial signs of cleidocranial dysplasia, Int. J. Paediatr. Dent. 14 (2004) 49–53.
[27] A. Saito, A. Ooki, T. Nakamura, S. Onodera, K. Hayashi, D. Hasegawa, T. Okudaira, K. Watanabe, H. Kato, T. Onda, A. Watanabe, K. Kosaki, K. Nishimura, M. Ohtaka, M. Nakanishi, T. Sakamoto, A. Yamaguchi, K. Sueishi, T. Azuma, Targeted reversion of induced pluripotent stem cells from patients with human cleidocranial dysplasia improves bone regeneration in a rat calvarial bone defect model, Stem. Cell Res. Ther. 9 (2018) 12.
[28] S. Onodera, A. Saito, D. Hasegawa, N. Morita, K. Watanabe, T. Nomura, T. Shibahara, S. Ohba, A. Yamaguchi, T. Azuma, Multi-layered mutation in hedgehog-related genes in Gorlin syndrome may affect the phenotype, PLoS One 12 (2017) e0184702.
[29] J. Pratap, M. Galindo, S.K. Zaidi, D. Vradii, B.M. Bhat, J.A. Robinson, J.Y. Choi, T. Komori, J.L. Stein, J.B. Lian, G.S. Stein, A.J. van Wijnen, Cell growth regulatory role of Runx2 during proliferative expansion of preosteoblasts, Cancer Res. 63 (2013) 5357–5362.
[30] S. Shibata, N. Suda, S. Yoda, H. Fukuoka, K. Ohyama, Y. Yamashita, T. Komori, Runx2-deficient mice lack mandibular condylar cartilage and have deformed Meckel's cartilage, Anat. Embryol. 208 (2004) 273–280.
[31] K. Nakashima, X. Zhou, G. Kunkel, Z. Zhang, J.M. Deng, R.R. Behringer, B. de Crombrugghe, The novel zinc finger-containing transcription factor Osterix is required for osteoblast differentiation and bone formation, Cell 108 (2002) 17–29.
[32] T. Liu, Y. Gao, K. Sakamoto, T. Minamizato, K. Furukawa, T. Tsukazaki, Y. Shibata, K. Bessho, T. Komori, A. Yamaguchi, BMP-2 promotes differentiation of osteoblasts and chondroblasts in Runx2-deficient cell lines, J. Cell. Physiol. 211 (207) (2007) 728–735.

[33] T. Matsubara, K. Kida, A. Yamaguchi, K. Hata, F. Ichida, H. Meguro, H. Aburatani, R. Nishimura, T. Yoneda, BMP2 regulates Osterix through Msx2 and Runx2 during osteoblast differentiation, J. Biol. Chem. 283 (2008) 29119–29125.
[34] J. Jing, R.J. Hinton, Y. Jing, Y. Liu, X. Zhou, J.Q. Feng, Osterix couples chondrogenesis and osteogenesis in post-natal condylar growth, J. Dent. Res. 93 (2014) 1014–1021.
[35] Y. Katori, J.F. Rodríguez-Vázquez, T. Kawase, G. Murakami, B.H. Cho, S. Abe, Early fetal development of hard tissue pulleys for the human superior oblique and tensor veli palatini muscles, Ann. Anat. 193 (2011) 127–133.
[36] M. Nara, K. Kitamura, M. Yamamoto, R. Nagakura, K. Mitomo, S. Matsunaga, S. Abe, Developmental mechanism of muscle-tendon-bone complex in the fetal soft palate, Arch. Oral Biol. 82 (2017) 71–78.
[37] C.M. Pereira, V.F. Alves, P.F. Gasparetto, R.C.N. Souza, T.L. Botelho, Cleidocranial dysplasia associated with the Dentigerous cyst: review of the literature and report of the clinical case, J. Health Sci. Inst. 28 (2010) 137–139.